Carderock Division, Naval Surface Warfare Center
West Bethesda, Maryland 20817-5700

CRDKNSWC/HD-1205-02 December 1997

Hydromechanics Directorate
Research and Development Report

BLADE SECTION LIFT COEFFICIENTS FOR PROPELLERS AT EXTREME OFF-DESIGN CONDITIONS

By

Young Shen
Donald Fuhs

CRDKNSWC/HD-1205-02 BLADE SECTION LIFT COEFFICIENTS FOR PROPELLERS AT EXTREME OFF-DESIGN CONDITIONS

REPORT DOCUMENTATION PAGE

Form Approved
OMB No. 0704-0188

1. AGENCY USE ONLY (Leave blank)	2. REPORT DATE	3. REPORT TYPE AND DATES COVERED
	December 1997	Research and Development, Oct 96 to Sept 97

4. TITLE AND SUBTITLE

Blade Section Lift Coefficients for Propellers at Extreme Off-Design Conditions

5. FUNDING NUMBERS

6. AUTHOR(S)

Young Shen and Donald Fuhs

7. PERFORMING ORGANIZATION NAME(S) AND ADDRESS(ES)

Hydromechanics Directorate, Code 5400
Carderock Division
Naval Surface Warfare Center
9500 MacArthur Boulevard
West Bethesda, MD 20817-5700

8. PERFORMING ORGANIZATION REPORT NUMBER

CRDKNSWC/HD-1205-02

9. SPONSORING/MONITORING AGENCY NAME(S) AND ADDRESS(ES)

Office of Naval Research
Ship Structures and Systems
S&T Division 334
800 N. Quincy Street
Arlington, VA 22217

10. SPONSORING/MONITORING AGENCY REPORT NUMBER

11. SUPPLEMENTARY NOTES

12a. DISTRIBUTION/AVAILABILITY STATEMENT

Approved for public release; distribution is unlimited.

12b. DISTRIBUTION CODE

13. ABSTRACT (Maximum 200 words)

The Propeller Force Module (PFM) code developed by Analytical Methods Inc. (AMI) for calculating propeller side forces during maneuvering simulation studies requires inputs of propeller blade sectional lift, drag, and moment data. A set of steady two-dimensional foil force data for NACA profiles is normally used by PFM as input. Wake survey data show that the propeller blade sections will encounter large spatial variations in angle of attack during maneuvers. A literature search is conducted to review the effect of unsteady angle of attack fluctuations on two-dimensional hydrodynamic forces. Methods to calculate unsteady hydrodynamic loads are evaluated, and a method selected for use with the PFM code.

14. SUBJECT TERMS

Propellers, foils, blade sections, unsteady forces, dynamic stall, stall hysteresis, lift, drag, pitching moment

15. NUMBER OF PAGES

34

16. PRICE CODE

17. SECURITY CLASSIFICATION OF REPORT	18. SECURITY CLASSIFICATION OF THIS PAGE	19. SECURITY CLASSIFICATION OF ABSTRACT	20. LIMITATION OF ABSTRACT
UNCLASSIFIED	UNCLASSIFIED	UNCLASSIFIED	

CONTENTS

FIGURES

TABLES

NOMENCLATURE

A_1, A_2, b_1, b_2	coefficients used in approximation to Wagner's function, Eq (7)
c	blade section local chord length
C_L	lift coefficient
C_{Lmax}	maximum lift coefficient
C_{Lmin}	minimum lift coefficient
C_{Lss}	lift coefficient at static stall
C_{L_α}	lift curve slope
C_{Nmax}	maximum normal force coefficient
C_{Nmin}	minimum normal force coefficient
C_P	pressure coefficient
k	reduced frequency, $\omega c/2V$
r	non-dimensional pitch rate $r=\alpha' c/2V$, Eq (15)
R	propeller radius
s	non-dimensional time parameter, $s=2Vt/c$, Eq (6)
Δs	non-dimensional time increment, see Eq (13)
t	dimensional time
Δt	dimensional time increment
V	reference velocity
X_n	a parameter used to compute the delay in angle of attack, see Eqs (10) and (11a)
Y_n	a parameter used to compute the delay in angle of attack, see Eqs (10) and (11b)
α	angle of attack
α'	rate of change of angle of attack
α_{att}	angle of attack when the flow reattaches
α_{fs}	angle of attack when the flow becomes fully separated
α_{DL}	dynamic lift divergence angle (angle of attack at Point 4), see Eq (21)
α_{DM}	dynamic moment stall angle (angle of attack at Point 3), see Eq (18)
α_{max}	maximum angle of attack to be encountered by the foil
α_{min}	minimum angle of attack to be encountered by the foil

$\alpha(0)$	initial angle of attack, see Eq (9)
α_{ss}	static stall angle of attack
$\Delta\alpha$	stall delay angle due to unsteady motion see Eq (18)
$\Delta\alpha_i$	step increment in foil angle for i^{th} time step used in Eq (10)
η	a parameter to relate lift and angle of attack, see Eq (1)
σ	cavitation number (negative pressure coefficient) in a fully separated flow, see Eq (3a)
Φ	Wagner's function, approximated by Eq (7)
Ψ	azimuth angle in the transverse plane
ω	oscillation frequency
Ω	propeller rotational speed in rad/sec

ABSTRACT

The Propeller Force Module (PFM) code developed by Analytical Methods Inc. (AMI) for calculating propeller side forces during maneuvering simulation studies requires inputs of propeller blade sectional lift, drag, and moment data. A set of steady two-dimensional foil force data for NACA profiles is normally used by PFM as input. Wake survey data show that the propeller blade sections will encounter large spatial variations in angle of attack during maneuvers. A literature search is conducted to review the effect of unsteady angle of attack fluctuations on two-dimensional hydrodynamic forces. Methods to calculate unsteady hydrodynamic loads are evaluated, and a method selected for use with the PFM code.

ADMINISTRATIVE INFORMATION

The work described in this report was performed by the Propulsor Department of the Hydromechanics Directorate, Carderock Division, Naval Surface Warfare Center. The work was sponsored by the Office of Naval Research, Ship Structures and Systems S&T Division (Code 334), under the Advanced Propulsor Task and the Maneuvering and Control Task of the FY97 Submarine Hull, Mechanical, and Electrical Technology Program (PE0602121N).

INTRODUCTION

A method is needed to predict the side forces and moments on marine propellers during extreme maneuvers, such as hard turns and crashback. The method must be capable of predicting propeller loads for large off-design angles of attack where stall may be occurring. The method must also be capable of running in real time for computer simulations used to train ship operators.

The most promising method to predict maneuvering forces for propellers is the Propeller Force Module (PFM) developed by Analytical Methods Inc. (AMI). The PFM is a blade element code that executes quickly because the blade section lift, drag, and pitching moment coefficients are determined off-line and stored in a look-up table. The user can input section coefficients based on measurements for angles of attack beyond stall and for reverse flow conditions that occur during crashback*. PFM is a quasi-steady code, and helicopter experience has shown unsteady effects are significant even for the low reduced frequencies of interest, $\alpha' c/2V < 0.6$ for shaft frequency. (Data for helicopters typically are $\alpha' c/2V < 0.2$). Therefore, it is considered necessary to develop a method to predict unsteady effects on blade section coefficients for extreme off-design conditions.

With the propeller operating behind a ship stern, the propeller blade sections will encounter different inflow angles onto the propeller blades at different azimuth angles due to

* Jiang, C.W., "Foil Sectional Lift, Drag and Moment Coefficients Prepared for Propeller Module Input", Memorandum, December 1996.

the spatial variation in ship hull wake. Maneuvering conditions change further the ship wake in the propeller plane. As an example, Fig 1 shows a typical inflow angle distribution on a blade section near the propeller radius r/R = 0.4 in a mild turn. The horizontal axis denotes the azimuth angle ψ in the circumferential plane. The vertical axis denotes the distribution of inflow angle in the circumferential plane. The angle of attack is roughly approximated by the difference between blade pitch angle and nominal advance angle (ϕ-β). Large spatial variations in angle of attack are shown in Fig 1. In some cases as much as 20 to 30 degree variations in inflow angle can be expected. Qualitatively, Fig 1 indicates that with a rapid variation in inflow angle across the blade sections the unsteady effects on propeller forces may not be small. The objective of this work is to construct unsteady sectional force data for input to the PFM code that includes potentially important unsteady effects.

An important consideration in the development of any hydrodynamic prediction method is its use in conjunction with other calculations in the simulation code. Simulations require predicting hull forces and moments and propeller inflow as well as propeller forces. If the dynamic stall prediction method is a frequently accessed subroutine in PFM code, then it should not have large computational requirements. This objective can be met by using semi-empirical dynamic models that rely on the reconstruction of the important dynamic flow features. A RANS code should be used to continuously improve the semi-empirical model.

Time scale is the major physical parameter in a dynamic model to distinguish itself from a static model. All other parameters influencing the force characteristics are expected to be similar in both models. It is shown in this report that the study of dynamic forces can be treated from an extension of the static forces. Static data will be used extensively in this dynamic model. This report will start with a brief review of static force characteristics including the effect of static stall and flow separation.

STATIC FORCES

The most important flow parameter governing the force characteristics of a lifting surface is the inflow angle, namely the angle of attack. The lift, drag and pitching moment coefficients are typically plotted in terms of angle of attack [1]. Basically, a cambered foil and a symmetric foil have the same force characteristics except the shift in the angle of zero lift due to the camber [1, 2]. Thus to first order, the following discussions are expected to be applicable to both symmetric and non-symmetric foils.

ATTACHED FLOW

Aerodynamic potential flow theory shows that the lift slope of a thin airfoil with fully attached flow is 2π per radian or 0.11 per degree. To incorporate the influence of finite thickness and fluid viscosity, the lift coefficient C_L and the section angle of attack, α are related by

$$C_L = 2\pi \alpha \eta \qquad \text{fully attached flow} \qquad (1)$$

where η is a quantity depending on the profile thickness and Reynolds number. A non-linear potential flow theory [2] shows that the lift slope increases with foil thickness which gives $\eta>1$. In a real fluid, asymmetry of the boundary layer tends to reduce η. A thick foil is more susceptible to flow separation that also reduces η.

Fig 2 shows the lift and drag characteristics of the NACA 0012 profile [3]. This set of data has been used in PFM sample runs, and has been used extensively in Ref 1, so it will be briefly discussed. The horizontal axis denotes the angle of attack raging from 0 to 180 deg. In the case of 180 deg, the foil was tested astern, namely the flow approached the foil from the trailing edge. In the forward tests (ahead), the lift force increases linearly with foil angle up to around 14 deg with the flow on the foil surface fully attached. The lift slope is found to be around 0.102 per deg which is 93% of 2π per radian, namely $\eta = 0.93$. In the reversed flow tests (astern), the lift force (negative) again increases linearly from 180 to 172 deg (0 to 8 deg). The lift slope is found to be 0.105 per deg which is 94% of 2π per radian, namely $\eta = 0.94$. The lift slopes are almost the same in both ahead and astern tests. Experimental data available in the literature show that Eq (1) can be used to calculate lift coefficients with η in the order of 0.93 to 1.0. At high Reynolds number cases, $\eta = 1$ can be used to give good results.

Note that in the forward tests (ahead), the foil leading edge is rounded and relatively thick. In the reversed flow tests (astern), the foil leading edge is sharp and thin. Test results show that (1) as long as the flow is fully attached, the lift characteristics are not sensitive to the leading edge profile; (2) however, the stall angle is extremely sensitive to the leading edge profile. In the forward tests with a rounded leading edge, the static stall angle α_{ss} is found to be around 14 deg. In the astern tests with a sharp leading edge, the static stall angle is found to be around 8 deg.

STATIC STALL

As shown in Fig 2, lift force increases linearly with the foil angle. However, at a certain foil angle, the boundary layer on the foil surface may grow too thick for the flow to remain fully attached. Flow separated from the foil surface will result in a substantial reduction in lift force due to modification of the Kutta condition. The foil is now in stall and the angle is denoted by the static stall angle α_{ss}. There are two types of stall. A trailing edge stall is associated with a thick foil. The trailing edge stall occurs when the pressure gradient in the pressure recovery region is too steep and the flow in the boundary layer is separated from the trailing edge. The growth of the separation zone and the drop in lift are gentle and gradual with the increase of the foil angle. On the other hand, leading edge stall is associated with flow separation near the leading edge. At a large foil angle the adverse pressure gradient around the leading edge may be so large that the flow separates from the leading edge. With the presence of a large adverse pressure gradient, the laminar separation bubble can grow so fast that the surface pressure is greatly modified with a sharp drop in lift force once the foil experiences leading edge stall. The change in forces with foil angle differs markedly between these two types of stall. The type of stall characteristics that occurs depends on the leading and trailing edge profiles, foil thickness,

camber, and Reynolds number. Eight different profiles have been investigated by McCroskey [4]. The NACA 0012 profile was shown to be associated with leading edge stall.

SEPARATED FLOW

Consider Fig 2a again. If the foil angle is greater than α_{ss}, the lift experiences a sharp drop from the maximum static lift. A further increase in the foil angle results in the boundary layer separating completely from the foil surface. The foil is in a fully separated flow regime. Let α_{fs} denote the foil angle for flow to become fully separated. In the fully separated flow regime the lift coefficients are seen to vary almost linearly with the foil angles between 20 to 35 deg in ahead and 156 to 147 deg (24 to 33 deg) in astern tests. The lift slopes are found to be 0.029 to 0.030 per deg for ahead tests and 0.030 to 0.032 per deg for astern tests. The lift slope on a foil with a sharp leading edge seems to give a slightly higher value than the foil with a rounded leading edge. It is also noted that the lift slope is substantially lower in a fully separated flow than in a fully attached flow.

The characteristics of a two-dimensional inclined flat plate at zero cavitation number have been obtained by Kirchhoff and Rayleigh. (See Ref 5). The resultant force on the plate is given by

$$C_N = \frac{2\pi \sin\alpha}{4 + \pi \sin\alpha} \qquad (2)$$

The pressure inside of the cavity is generally not zero. Let σ denote the non-dimensional pressure inside the cavity and given by

$$\sigma = -C_p = (P_o - P)/0.5\,\rho\,V^2 \qquad (3a)$$

where P and P_o denote cavity pressure and reference pressure, respectively. For small values of σ the lift coefficient C_L is given by [5]

$$C_L = \frac{2\pi \sin\alpha}{4 + \pi \sin\alpha}\,[1 + \sigma + \sigma^2/(8(\pi+4))]\cos\alpha \qquad (3b)$$

Vorticity in the wake has been studied by Fage and Johansen on an inclined flat plate [see Ref 5]. They also have measured the pressure distributions on the upper and lower surfaces of the plate at various angles of attack as shown in Fig 3. Pressure distribution data show that at the foil angles greater than 14.85 deg, the flow on the foil surface is fully separated. The measured pressure inside the fully separated flow for various foil angles is given in Table 1.

Table 1. Pressure inside a separated flow.

α (deg)	90	70	50	30	15
σ	1.380	1.360	1.230	0.924	0.622

As an example, the lift coefficient at 30 deg angle of attack can be calculated by

$$C_L = \frac{2\pi \sin 30}{4 + \pi \sin 30} [1 + 0.924 + (0.924)^2/(8(\pi+4))] \cos 30$$

$$= 0.94$$

Consider Fig 2a again of the NACA 0012 profile. The measured and computed C_L values are given in Table 2 for comparison.

Table 2. Measured and Computed Lift Coefficients for NACA 0012 [3].

α^o	σ	**Measured C_L**	**Calculated C_L**
20	0.72	0.68	0.68
30	0.924	0.98	0.94
50	1.230	1.1	1.09
70	1.360	0.71	0.69
90	1.380	0.10	0.0
150	0.924	-0.94	-0.95
155	0.83	-0.77	-0.82

The measured lift coefficients are well predicted by Eq (3). This equation will be used to calculate the forces in a separated flow. In this respect, the drag coefficients can be calculated by

$$C_D = \frac{2\pi \sin \alpha}{4 + \pi \sin \alpha} [1 + \sigma + \sigma^2/(8(\pi+4))] \sin \alpha \qquad (4)$$

The measured and computed C_D values are given in Table 3 for comparison.

Table 3. Measured and Computed Drag Coefficients for NACA 0012 [3].

α^{o}	σ	Measured C_D	Calculated C_D
20	0.72	0.26	0.25
30	0.924	0.58	0.55
50	1.230	1.0	1.30
70	1.360	1.85	1.91
90	1.380	2.03-2.07	2.12
150	0.924	0.66	0.55
155	0.83	0.43	0.39

The static stall angle is an important parameter that divides the flow into two regimes with different lift slopes and methods of calculation. Similarly the dynamic stall angle is expected to exert important effect on the dynamic forces. As to be shown in the subsequent sections, the dynamic force manifests itself from the static force through the effect of time scale. All the other physical parameters are likely to be insensitive to the time scale. Namely aside from difference in the values of stall angle, the dynamic and static forces in terms of foil angles will exhibit similar characteristics. To the first approximation, the present dynamic model assumes that the effects of foil geometry and Reynolds number on dynamic force are small. This assumption leads to the extensive use of static data in constructing a dynamic stall model.

UNSTEADY FORCES

DYNAMIC FORCE CHARACTERISTICS

A ship propeller sees incoming vorticity from the hull and appendage wakes, and the vorticity is distorted as it is convected through the blade passages. This is essentially a gust type of problem. However, there are no dynamic stall measurements available for stationary marine propeller blade sections in a gust for the range of reduced frequencies and angles of attack of interest, or for reversed flow. Most isolated airfoil data on dynamic stall is for helicopter section shapes with oscillating pitch in uniform flow. For the low reduced frequencies of interest, Sears function and Theodorsen functions are approximately the same since the first harmonic wave length is long compared to the chord length. Therefore, data for oscillating pitch foils is considered to be of value for evaluating dynamic stall on sections with constant pitch experiencing oscillating angles of attack.

The AMI PFM code is based on the assumption that each blade section acts as an isolated two-dimensional foil. It is intended to assess more complicated effects such as cascade effects, the unsteady effective wake problem, and three-dimensional effects such as aspect ratio corrections and sweep effects after the simpler isolated foil method has been implemented and evaluated.

Extensive unsteady experimental works have been conducted on a sinusoidal motion such as pitching oscillation, heaving oscillation, and gust [6, 7], because of the relative

simplicity in characterizing the unsteady motion. In a few occasions the experiments have been carried out for a transient motion [8, 9]. Fig 4 shows an example of force measurements in a sinusoidal pitching oscillation [10]. The instantaneous angle of attack α is given by

$$\alpha = \alpha_0 + \Delta\alpha \, \text{Sin} \, \omega t \tag{5}$$

In this example, the foil was tested at a mean foil angle of α_0 =15 deg and an oscillation amplitude of $\Delta\alpha$ =10 deg at a reduced frequency of k=0.10. This test gave the maximum angle of α_{max} =25 deg and minimum angle of α_{min} = 5 deg. The measured dynamic data are plotted in a solid line. The static data are also given in the same figure in a dashed line.

Numbers are marked in this figure to illustrate the basic characteristics of dynamic response. At Point 1, the flow on the foil surface is fully attached. The dynamic lift slope is almost the same as the static value; namely the unsteady and steady data are overlapped in this flow regime. The foil experienced static stall around α_{ss} =12 deg. Under the oscillation condition, the lift coefficient continues to exhibit a linear relationship with α up to around 17 deg. Experimental data indicate that the unsteady effect on lift slope is small. On the other hand, the dynamic lift stall angle is greatly delayed by the unsteady motion.

The physical phenomenon observed in the dynamic stall can be explained from the relationship between the boundary layer separation and the adverse pressure gradient. Fig 5 shows an example of pressure distributions on the foil surface at a steady and unsteady condition [11]. Unsteady motion is seen to reduce the leading edge suction pressure peak; and the adverse pressure gradient is reduced. By using the Theodorsen function, Carta [11] shows that under the unsteady motion the separation bubble moves against the adverse pressure gradient without separating the boundary layer until well beyond the steady stall angle. In this respect, a significant delay in the occurrence of cavitation inception due to unsteady motion has also been observed in pitching foil experiments investigated by Shen and Peterson [12]. The measured intensity of suction pressure peak at the leading edge is greatly reduced with the increase of oscillation frequencies. The foil angles to exhibit cavitation inception are delayed.

Fig 6 shows the effects of oscillation amplitude on the unsteady pressure distribution [13]. In this series of tests the foil mean angle remained at 7 deg but oscillation amplitudes were varied from 0.5 to 2.0 deg. The increase in oscillation amplitude is also seen to reduce the intensity of suction pressure peak around the leading edge. Frequency and oscillation amplitude are the two most important parameters governing the dynamic response.

Consider Fig 4 again between Point 1 to Point 2. Experimental data indicate that a thin attached boundary layer continues to exist up to Point 2. This gives a linear relationship between the dynamic lift and the foil angle well above the static stall angle. In the initial dynamic model, it is assumed that the lift slope under the unsteady motion remains the same as in the steady case. The lift slope measured or calculated from the static tests will be used extensively in the dynamic model. It is implicitly assumed in this semi-empirical model that the section profile geometry and Reynolds number have the same effect on steady and unsteady forces as long as a thin attached boundary layer is maintained on the foil surface. In

the second phase of dynamic modeling the possible effect of camber, leading edge profile and Reynolds number due to unsteady motion needs must be evaluated to improve the first generation model.

Force characteristics between Point 2 to Point 3: When the foil angle reaches Point 2, the foil will start to experience flow reversal. A stall vortex starts to appear around the foil leading edge [10, 14]. However, experiments indicate that the lift force is still not affected by the appearance of flow reversal. The lift slope can be linearly extended from Point 2 to Point 3. However, it is remarked that due to the unsteady motion there is a phase shift between forces and angles. The effect of time scale on forces will be included in unsteady force calculations.

Force characteristics between Point 3 to Point 4: When the foil angle reaches Point 3, the stall vortex begins to detach from the leading edge and is convected downstream. The pressure distribution on the foil surface is markedly modified by the detached stall vortex [15, 16]. The lift curve starts to exhibit some nonlinear behavior beyond Point 3. The moment curve starts to diverge from the static value and the form drag increases markedly. The foil angle at Point 3 is termed dynamic moment stall angle α_{Dm}.

When the foil angle exceeds Point 3, the strength of the stall vortex is intensified. The low pressure induced by the stall vortex moves further aft with the increase of reduced frequencies [8, 13]. The delay in the occurrence of stall and the sustained upper surface suction pressure associated with the chordwise passage of the coherent vorticity shed during the stall process will result in a significant increase in the unsteady lift force over the maximum static force. The lift slope is expected to increase substantially. A method to calculate the unsteady force will be presented later.

Force characteristics between Point 4 to Point 5: A maximum lift is attained at Point 4 when the stall vortex is approaching the trailing edge with the flow on the upper surface in the verge of becoming fully separated. The form drag is a maximum at Point 4. The center of pressure moves rearward resulting in a sharp drop in the moment coefficient. When the foil angle exceeds Point 4, the lift drops sharply from the maximum value. The foil angle at Point 4 is termed dynamic lift stall angle α_{DL}. When the foil angle exceeds Point 4, the stall vortex passes across the trailing edge. The flow on the upper surface becomes fully separated. The lift force takes a sharp drop with an increase in foil angle. This is a case corresponding to the type of leading edge stall. In some instances, a secondary vortex may appear. In this respect cavitating hydrofoil experiments exhibit a similar phenomenon. The cavity interface is a free shear layer [12, 17]. When the cavity length reaches the trailing edge of the foil the free shear layer becomes very unstable. The cavitating hydrofoil experiences buffeting similar to the fluctuating lift force exerted by the secondary vortex in the noncavitating oscillating airfoil tests. Generally the buffeting phenomenon only lasts a relatively short time. In the present dynamic model the possible effects of a secondary vortex on forces is not considered.

Force characteristics between Point 5 to Point 6: the strength of the stall vortex is diminishing when the foil angle begins to recess. Initially the foil surface remains fully separated. At Point 6 the foil angle becomes so small that the stall vortex disappears. The

separated flow begins to reattach itself on the foil surface. The lift force readjusts itself to the linear regime with a further reduction in the foil angle.

When the flow begins to reattach at Point 6, the unsteady lift coefficient $C_L = 1.0$ is much lower than the static stall $C_{Lmax} = 1.5$. The hysteresis loop reconnects to the static curve at $\alpha = 5$ deg, which is well below the static stall angle of $\alpha_{ss} = 12$ deg. For some foils, the lift hysteresis loop forms a figure 8 shape instead of the triangular shape shown at the top of Fig 4.

Fig 7 shows another example of a pitching foil experiment [18]. The static force data are also plotted in Fig 7. The oscillation test was conducted at a mean angle of 24.57 deg, the oscillating amplitude of 4.85 deg, and the reduced frequency of 0.124. This test condition gives $\alpha_{min} = 19.72$ deg. From the static data, it is clear that the foil has remained in full separation throughout the whole cycle of oscillation. The test result shows that in a fully separated flow regime, the values of lift slope are nearly the same for both steady and unsteady tests. This result supports the assumption given in the introduction that the dynamic force can be treated as an extension of the static force in either fully wetted or fully separated flow regimes. It is assumed that the lift measured in steady tests or computed from Eq (3b) can be used in the unsteady model when the foil is fully separated. However, it is remarked that due to the unsteady motion there is a phase shift between forces and angles. The effect of time scale on forces will be included in unsteady force calculations.

As shown in Fig 1, a typical inflow angle distribution on a blade section at propeller radius $r/R = 0.4$ does not behave sinusoidally. The effect of transient motion on forces in respond to a ramp change in angle of attack has been investigated by Ham and Garelick [8] and others [14, 15]. A comparison of transient and sinusoidal motion data shows that the delay in dynamic stall angle and the attainable maximum dynamic lift are more pronounced in the transient case than in a sinusoidal motion. The maximum dynamic lift for the transient case is 3 times the maximum static lift.

Oscillating experiments indicate that the foil total circulation never achieves its potential value, and therefore the leading edge vorticity shed during repeated foil oscillation is less intense than would be if the foil had time to unstall completely during the cycle [19]. This is a reason that the loads observed during an oscillatory motion of an airfoil are noticeably lower than the loads encountered during a transient motion. This result indicates that the oscillating foil data must be used with care in constructing a dynamic model.

UNSTEADY FORCE CALCULATIONS

In simulation studies for maneuvering, the distribution of inflow angles around the propeller circumference is computed first. The rate of change in inflow angle is next computed. The forces associated with the instantaneous angle of attack as shown in Fig 1 are then computed. It is necessary to iterate because the induced velocity and thus the angle of attack depend on the magnitude of the computed forces, and the computation of the forces requires knowing the angles of attack.

A dynamic stall model can be divided into a few flow regimes as discussed previously. A thin attached boundary layer regime exists for the foil angle up to Point 3. A detached stall vortex regime for the foil angle exists from Point 3 to Point 4. A transition regime exists from partial to full separation between Point 4 to Point 5. A fully separated flow regime exists for the foil angle from Point 5 to Point 6. A transition regime exists from fully separated to attached flow between Point 6 to Point 1. A different computational method is required to relate forces and foil angles in each flow regime.

Attached Thin Boundary Layer Flow Regime Up to Point 3

Theories to compute unsteady hydrodynamic forces have been developed by Theodorsen for a foil in a sinusoidal pitching and heaving motion, by Sears for a foil in a sinusoidal transverse gust, and by Wagner for a step increase in angle of attack. These theories have been used quite extensively in aerodynamics for helicopter blade force calculations. However, in the present study, the change in inflow angle onto the propeller blades due to the ship wake is neither a sinusoidal variation nor a step increase. For attached flow, one could predict propeller steady side forces due to the first harmonic of wake. However, stall is a response to all harmonics of wake, not just the first harmonic. Therefore, it is necessary to consider all harmonics of wake when predicting the occurrence of stall.

According to the principle of linear superposition, arbitrary transient loads can be treated as a sum of elementary functions. One could take the Fourier transform of the velocity component normal to the blade chord line, apply Sears function to each harmonic, and then take the inverse transform to sum the contributions of all harmonics. This approach of taking transforms and inverse transforms each time the wake changes is probably too time-consuming for real time simulations. Gangwani [23] has developed a numerical time-stepping procedure that should execute more quickly. He treats arbitrary transient loads as a sum of step functions, by means of the Wagner function and LaPlace transforms. The analytical solution is expressed as a time integral which he solves using a time marching scheme that is second order accurate. Details of the method are given below.

Let s denote a non-dimensional time parameter given by

$$s = 2Vt/c \tag{6}$$

where V is the characteristic velocity, t is time and c is the propeller blade chord length. Physically, s denotes a streamwise distance in terms of a semi-chord. Wagner's step function [20] in response to a step change in angle of attack $\Delta\alpha$ can be approximated by [21, 22]

$$\Phi(s) = 1.0 - A_1 e^{-b_1 s} - A_2 e^{-b_2 s} \tag{7}$$

where A_1 =0.165, b_1 = 0.0455 , A_2 =0.335 , and b_2= 0.3. The numerical value of $\Phi(s)$ is shown in Fig 8. At time t = 0, $\Phi(0)$ = 0.5; namely only half of the lift due to the change $\Delta\alpha$ is generated by the foil at the initial instant of time. The full lift is produced only after the non-dimensional

time s is greater than approximately 30, namely after the foil has traveled more than 15 chord lengths. Time scale is seen to be very important in calculating the unsteady force.

The time-varying circulatory lift coefficient C_L (s) due to a step change in angle of attack, $\Delta\alpha$ can be expressed by

$$C_L(s) = C_L(0) + C_{L_\alpha}\,\Delta\alpha\Phi(s) = C_L(0) + C_{L_\alpha}\,\alpha_E(s) \tag{8}$$

where C_L (0) is the initial lift coefficient at time t=0, before the change of foil angle is initiated. C_{L_α} denotes the lift slope. It is assumed that the dynamic and static lift slopes have the same value; namely the static value will be used in the dynamic model. Physically, the term $\Delta\alpha\Phi(s)$ represents an effective angle of attack α_E.

For a two-dimensional airfoil going through an arbitrary change in angle of attack as noted in Fig 1, the instantaneous effective angle of attack can be described using Duhamel's integral function [20, 23, 35] given by

$$\alpha_E(s) = \alpha(0)\,\Phi(s) + \int_0^s (d\alpha/d\sigma)\,\Phi(s-\sigma)\,d\sigma \tag{9}$$

where $\alpha(0)$ corresponds to the initial angle of attack at time s = 0. By taking the LaPlace transform of Duhamel's integral function, Beddoes [21] and Gangwani [23] showed that the effective angle in a time series can be approximated by

$$\alpha_E(s_n) = \alpha(0) + \sum_{i=1}^{n} \Delta\alpha_i - X_n - Y_n \tag{10}$$

where

$$X_0 = 0 \quad \text{and} \quad X_n = X_{(n-1)}\,e^{-b_1\Delta s} + A_1\Delta\alpha_n \tag{11a}$$

and

$$Y_0 = 0 \quad \text{and} \quad Y_n = Y_{(n-1)}\,e^{-b_2\Delta s} + A_2\Delta\alpha_n \tag{11b}$$

The constants A_1, A_2, b_1, and b_2 are defined in Eq (7).

Consider Fig 1 again. Let Ω denote the propeller rotational speed in rad/sec. Let the azimuth angle ψ in the propeller plane to be expressed in degrees and t in seconds. Then,

$$\psi = \Omega\,(180/\pi)\,t \tag{12}$$

and the time increment Δs is given by

$$\Delta s = 2V\,\Delta t/c = 2V(\Delta\psi)\,(\pi/180\,\Omega)/c \tag{13}$$

The unsteady lift due to changes in angle of attack prior to stall can be computed from the angle of attack distribution such as that in Fig 1 and Eqs (8) to (13). This numerical approach converges readily to Theodorsen's analytical solution for a wide range of initial conditions and time step sizes, when the angle of attack varies sinusoidally with time. Eqs (8) to (11b) give the circulatory lift. Marine propellers tend to operate with higher reduced frequencies ($k<0.6$) than helicopters ($k<0.2$), and it is planned to modify the equations to account for added mass effects in the future. The formulation so far is based on a potential flow theory. It is assumed that the effects of profile geometry and Reynolds number on unsteady forces are incorporated in the $C_L(0)$ and C_{L_α} terms obtained from the static data. A RANS code should be used to improve this assumption.

Stall Vortex Detached Regime Between Points 3 and 4

The stall vortex detaches from the leading edge of the foil at Point 3 and approaches the trailing edge at Point 4. The coherent stall vortex induces additional suction pressure on the foil surface, especially at the rear part of the foil. This results in an increase in maximum attainable lift, dynamic lift slope, nose down pitching moment, and pressure drag. The theoretical treatment on the unsteady force in this regime is not yet available in the literature. Instead, the force calculation will be based on empirical formulas.

Dynamic Lift Slope Between Points 3 and 4.

An unsteady ramp test on a NACA 0012 airfoil section has been conducted by Ham and Garelick [8]. The change in angle of attack with time is given in Fig 9a. The averaged pitch rates in these four examples are 3.12, 13.68, 3.34, and 19.95 radians per second for the cases A, B, C, and D, respectively. The measured normal force coefficients are shown in Fig 9b. The normal force data is used to derive expressions for lift even though normal force and lift are approximately equal only for small to moderate angles of attack. In addition to the force measurements, 49 pressure transducers were installed on the foil to measure the surface pressure distributions. Consider the test case A. Inspection of the pressure distributions suggests that the stall vortex inception occurs around 17.9 deg and maximum lift occurs at 19 deg. The dynamic lift slope between the angles of 17.9 and 19 deg is around 0.165 per deg. Recall that the steady lift slope of a two-dimensional section in a fully attached flow is 2π per radian or 0.110 per deg. In the stall vortex regime, the dynamic lift slope of 0.165 is seen to be substantially greater than the static lift slope of 0.110 per deg. The dynamic lift slopes for the test cases B, C, and D are 0.185, 0.167, and 0.126 per deg , respectively. In this series of tests no systematic trend between dynamic lift slope and pitch rate has been observed.

Fig 10 shows another example of a cambered NACA 23012 wing section tested by Green et al [14]. The model was tested with a ramp-up motion from -1 to 40 deg. The inception of detached stall vortex occurs at the angle of attack of 27.5 deg. The foil attains the maximum lift at 33.5 deg, which is substantially higher than the static stall angle α_{ss} = 16.5 deg. This series of tests gives the dynamic lift slope of 0.186 per deg compared to the static lift slope of 0.105 per

deg. Green's result is in qualitative agreement with Ham and Garelick's data. Further information on Green's data for other wing sections is given in Ref [24]. Based on available experimental data the dynamic lift slope of 0.165 per deg or 3.0 π per radian is selected to calculate the dynamic loads between Points 3 and 4, namely

$$C_L(s) = C_L(\alpha_{Dm}) + (\alpha - \alpha_{Dm}) C_{L_\alpha} \Phi(s) \qquad \text{for } \alpha_{Dm} < \alpha < \alpha_{DL} \tag{14}$$

where $C_L(\alpha_{Dm})$ is the lift coefficient at Point 3

$C_{L_\alpha} \Phi(s)$ is approximately 3.0 π per radian

In Eq (14), the dynamic lift slope is treated as a quasi-steady slope C_{L_α} multiplied by an unsteady function such as the Wagner function $\Phi(s)$.

Maximum Dynamic Lift at Point 4

The magnitude of the adverse pressure gradient on a given foil is sensitive to the reduced frequency, and so is the maximum attainable lift force. Let α' denote the rate of change of angle of attack. In the present study, the dimensional unit of α' will be in radian per second. Let r denote the non-dimensional reduced pitch rate in the transient motion and represented by

$$r = \alpha' c/2V \qquad \text{in radians} \tag{15}$$

Oscillation motion. Johnson [25, 26] has used a set of oscillating foil experiments given in Fig 11 to obtain an empirical formula for the maximum dynamic lift coefficient and minimum moment coefficient at Point 4 for a sinusoidal motion as follows.

$$C_{Lmax} = \begin{cases} C_{Lss} + 80\,(\alpha' c/2V) & \alpha' c/2V < 0.025 \\ C_{Lss} + 2.0 & \alpha' c/2V > 0.025 \end{cases} \tag{16}$$

where C_{Lss} denotes the lift coefficient at static stall. Johnson assumes that when the lift coefficient reaches a maximum value of 3.0, the lift coefficient then remains at 3.0 as long as the foil angle is still rising, as seen in Fig 11. In the present dynamic model, C_{Lss} will be obtained from the measured static data.

Ramp Motion. Ramp tests by Green and Galbraith [14] are shown in Fig 12 which indicates that the maximum lift coefficient reaches 3.5 at r = 0.026 before a constant lift coefficient is observed. This result agrees with the previous discussions that the effect of dynamic forces from a ramp motion is stronger than from a sinusoidal motion. However, the pitch rate to reach a maximum lift coefficient is seen to be insensitive with the type of motion. In the ramp tests it is r = 0.026, whereas in the sinusoidal tests it is r = 0.025. From Fig 12, the maximum dynamic lift coefficient in a ramp motion is obtained by

$$C_{Lmax} = \begin{cases} C_{Lss} + 92\,(\alpha'\, c/2V) & \alpha'\, c/2V < 0.026 \\ C_{Lss} + 2.4 & \alpha'\, c/2V > 0.026 \end{cases} \qquad (17)$$

Another series of ramp tests with a suddenly increased angle of attack has been conducted by Kramer [9] with three wing models and two Reynolds numbers. The models consisted of two symmetric and one non-symmetric wing section. Kramer's data only cover low pitch rates. Within the test matrix, the measured maximum lift is also found to vary linearly with the pitch rate.

Flow Transition Regime Between Points 4 and 5: Once the stall vortex passes the trailing edge, the lift force drops markedly from Point 4 to Point 5. The dynamic stall should exist for a definite time, regardless of the subsequent blade motion. Therefore, the fully separated flow regime is assumed not to start until at least a short time after the dynamic stall angle is reached, if the angle is still increasing after this point. Johnson [25, 26] assumes that dynamic stall extends only for the circumferential angle of about $\Delta\psi = 15$ deg namely, within this period of time the maximum lift drops straight to the static fully separated value. However, the fully separated flow regime begins when the angle starts to decrease.

Forces in a Fully Separated Flow Regime Between Points 5 and 6. Fig 13 shows the force response in a ramp-down test on a NACA 0015 section [27]. The foil angle was reduced from + 40 deg to -1 deg at the pitch rates of r = - 0.003 to - 0.033. The minus sign indicates ramp-down tests. When the angle was reduced to around 17 deg, flow attachment occurred for the test case of r =-0.003. This foil angle is termed incidence of flow attachment and is denoted by α_{att} at Point 6. The corresponding lift (normal) force exhibits a local minimum, $C_{N\,min}$. A further decrease in foil angle results in an increase in lift force due to an increase in suction pressure associated with attached flow.

Fig 13 shows that the lift slope in a fully separated flow regime is not significantly altered by the pitch rate. The lift curves at various pitching rates appear in a small cluster. As a first approximation, the static lift slope measured in the fully separated flow regime or computed from Eq (3b) will be used in the dynamic model. However, in the dynamic case, the dynamic response is influenced by the time scale due to the effect of phase shift that alters the relationship between forces and angles. Wagner's step function developed for a fully attached flow [20] will be applied to the fully separated flow. This assumption should be evaluated. In this respect the unsteady supercavitating flow theory developed by Widnall may be worthy of evaluation [28]. Fig 13 further shows that the occurrence of flow attachment, α_{att} is delayed with the increase in negative pitch rates. This is a reverse phenomenon of dynamic stall.

Forces in a Partially Attached Flow Regime Between Points 6 and 1. Force response from an airfoil in a re-attaching flow regime is very similar to the force response of a hydrofoil in a partially cavitating regime. Unsteady partially cavitating hydrofoils have been extensively investigated both theoretically and experimentally. The dynamic forces on a cavitating foil are found significantly affected by reduced frequency and the oscillating amplitude [12]. In the present application, similar to the dynamic stall phenomenon, the flow re-attaching is likely to take place in a short time as the foil angle is further reduced. Following Johnson's approach, it is assumed that the re-attaching extends only for circumferential angles of about $\Delta\psi = 15$ deg, and within this period of time the lift adjusts itself to the fully attached flow value. This assumption should be further evaluated in the second phase of study. The description of dynamic force calculations is completed. The next step is to quantify the boundary of various flow regimes for force calculations.

DYNAMIC STALL BOUNDARY

Dynamic Moment Stall Angle, α_{Dm}

As noted in Fig 4, the linear range of lift slope extends from Point 1 to Point 3. At Point 3 the stall vortex starts to detach from the leading edge, and the moment coefficient takes a divergence from the static value. The lift slope becomes non-linear at angles above Point 3. The unsteady force calculations given in Eqs (8) to (11) are applicable only up to Point 3. The dynamic moment stall angle, α_{Dm}, which is the angle of attack at Point 3, must be known in advance prior to performing the unsteady force calculations.

Pitching foil experiments [13] show that a major effect of foil motion is to reduce the amplitude of the suction pressure peak. The unsteady pressure gradient becomes less unfavorable than the steady pressure gradient. The separation bubble can move against the adverse pressure gradient without separating the boundary layer until well beyond the steady static stall angle. Let α_{Dm} denote the dynamic moment stall angle, expressed by

$$\alpha_{DM} = \alpha_{SS} + \Delta\alpha \tag{18}$$

where $\Delta\alpha$ denotes the moment stall delayed angle due to unsteady motion. The value of static stall angle α_{SS} is assumed known from Abbott and von Doenhoff [1]. Methods to estimate $\Delta\alpha$ will now be briefly discussed.

Theoretical Approach. The occurrence of static or dynamic stall is closely related to the adverse pressure gradient [13, 16]. Johnson and Ham [19] assume that the dynamic stall delay is the effect of change in the unsteady pressure gradient on the location of the transition point of the leading edge bubble. This assumption is verified experimentally when the dynamic stall angle is compared with the angle at which the bubble reattachment point passes the 15% chord station as seen in Fig 14. It was found that the delay in each angle due to pitch rate was almost identical. Based on the velocity and velocity gradient obtained from an unsteady thin airfoil theory, the pressure gradient and critical Reynolds number are related by the use of

Pohlhausen's shape factor. They further assume that the stall delay is linearly related to the forward movement of the transition point. Experimental data are introduced to determine two free parameters. The stall delay angle $\Delta\alpha$ is derived and given by

$$\Delta\alpha = \alpha_{ss} (\alpha' c/2v)(0.74 - 0.20\ ax)/0.03 \qquad (19)$$

where ax is the distance of the pitch axis from the leading edge normalized by the chord c. The symbol α' denotes the rate of change of foil angle of attack with time. The theoretical work has provided a reasonable physical explanation of dynamic stall delay due to the reduction of adverse pressure gradient but is not adequate to provide quantitative prediction when the experimental data are compared. In this respect Beddoes' work [21] also points out the possibility to construct a semi-empirical criterion to relate leading edge pressure gradient and dynamic stall.

Empirical Approaches. Several empirical formulas have been presented in the literature [23, 29, 30]. In addition to the reduced frequency and instantaneous angle of attack, Gangwani [23] assumes that dynamic stall phenomena in a transient motion can be characterized in a time domain by introducing a parameter α_w which accounts for the time history effects of the change in foil angle. Gangwani introduces a series of empirical parameters obtained from synthesized airfoil data. The magnitudes of parameters shown in Gangwani 's approach differ markedly among the different sets of test data. This fact makes it difficult to use Gangwani 's empirical coefficients in the present model.

Niven and Galbraith [15] have conducted dynamic tests on three symmetric foils of NACA 0012, 0015 and 0018 and four non-symmetric foils of NACA 23012 and trailing edge modification of NACA 23012 to investigate thickness and camber effects on the dynamic stall process. They observed that the onset of dynamic stall was closely related to the leading edge vortex inception. Using measurements from pressure sensors, Niven and Galbraith related the pressure variation (Cp) and the onset of the leading edge vortex. The dynamic stall onset incidence is taken to be the occurrence of the Cp divergence. Dynamic stall onset angles plotted against reduced pitch rates for three symmetric foils are shown in Fig 15a. The delay in dynamic stall inception angle is seen to be almost linear with the reduced pitch rate. The slopes are around 228, 302, and 272 deg per unit pitch rate for NACA 0012, 0015, and 0018, respectively. No systematic trend with thickness is noted. The effect of camber on dynamic stall onset is shown in Fig 15b. Again, dynamic stall inception angle is almost linear with pitch rate, with slopes of 300 and 233 for NACA 23012B and 23012C, respectively. The averaged value is around 267 for the symmetric and cambered foils. Gormont [32] expresses stall delay angle $\Delta\alpha$ by the square root of pitch rate. However, his conclusion that stall delay angle varies with the square root of pitch rate is uncertain because of scatter in the data he used.

Tran and Petot [31] introduced an additional pitch acceleration term in their dynamic stall model. Their data are limited to a small unsteady motion. None of the data attained the high value that has been observed to accompany the fully developed vortex-shedding phenomenon. The effect of the pitch acceleration term on stall delay is not considered further in this study.

There are some reports using another approach based on time delay constants to estimate the dynamic stall [21, 25, 33]. The response to a continuously varying angle of attack is constructed by treating the time history as an accumulating series of step functions. It is assumed that when the local value of angle of attack exceeds the static stall angle, the onset of flow separation is delayed for a finite period of time τ_M, during which the lift and moment behave as appropriate for attached flow. Different time constants have been introduced by Beddoes [21] and Johnson [25]. The time delay is insensitive to pitch rate, according to their approach.

Theoretical approaches to determine adequately the stall delay angle are not yet available, and experimental data on the time delay approach are relatively limited. Most of the test data seems to indicate that the stall delay angle follows closely in a linear relationship with the pitch rate. Niven and Galbraith data cover foils with different thickness and cambers. For the moment this set of data is selected to estimate the stall delay angle, using the following formula.

$$\Delta\alpha \text{ (deg)} = 267\, \alpha' c/2v \tag{20}$$

Dynamic Lift Divergence Angle, α_{DL}

Experiments indicate that foil lift achieves a maximum at Point 4 of Fig 4 when the dynamic stall vortex approaches the trailing edge of the foil [4, 23]. Discussions given in the previous section indicate that the dynamic lift slope is around 3π per radian or 0.165 per deg between Point 3 and Point 4. The peak lift coefficient approaches a universal constant of approximately 3.5 when the pitch rate is greater than 0.025 [15]. Let $C_L(\alpha_{DM})$ denote the lift coefficient at the dynamic moment stall angle α_{DM} (Point 3). The dynamic lift divergence angle, α_{DL}, which is the angle of attack at Point 4, can be estimated by

$$\alpha_{DL} = \alpha_{DM} + 6.06\, [C_{Lmax} - C_L\, (\alpha_{DM})] \qquad \text{in deg} \tag{21}$$

where

$$C_{Lmax} \leq 3.5$$

Following Johnson's approach, once the dynamic lift stall occurs and if the angle of attack is still increasing, the maximum lift coefficient is assumed to maintain at a constant value of 3.5.

Another approach to estimate the maximum lift angle. Experiments indicate that the maximum lift at Point 4 of Fig 4 is measured when the dynamic stall vortex reaches the trailing edge. If the stall vortex convection time is known, the dynamic lift stall angle can be estimated. Green et al [14] conducted a series of experiments on symmetric and cambered NACA foil models to measure the dynamic stall vortex convection speed. Test results indicate that to the first order of approximation the convection speed is independent of airfoil profiles and types of motion. Furthermore, the convection speed is found to be uniform across the chord and is in the order of $u/V = 0.36$, namely around 36% of the free stream velocity. The time required for the stall vortex to reach the trailing edge is then on the order of

$$t = C/0.36V \qquad (22)$$

From the pitch rate and convection time, the angle of attack to experience dynamic lift stall can be evaluated. This approach is also used by Gangwani to derive a semi-empirical formula for the dynamic stall model [23]. The empirical formula given in Eq (22) is much easier to apply and is recommended in this report.

Flow Reattachment Angle, α_{att}

Depending on the magnitudes of the instantaneous angle of attack, the foil can experience flow reattachment. Fig 16 shows an example of a NACA 0015 foil from a ramp down test with the foil angle reduced from 30 deg to 0 deg at several reduced pitch rates. [34]. The negative pitch rate indicates that the foil angle of attack decreases with time. Let C_{Nmin} denote the local minimum normal force as marked in the figure. The foil angle corresponding to C_{Nmin} is termed the flow reattachment angle, α_{att}. This is an important parameter as it indicates a rapid return to attached flow behavior, and marks the end of the separated flow response. Significant delay in reattached foil angle with pitch rate is noted.

Some similarity exists between airfoil flow separation and reattachment and hydrofoil cavitation and suppression. The physical phenomenon associated with unsteady separated flow and cavity flow is very complex. The theoretical treatment on this subject is still not available and experimental data are relatively scarce. Based on the limited experimental data, the flow reattachment angle will be estimated as follows.

Let $\tau = (\Delta t\, V)/c$ denote a non-dimensional time constant with V = free stream velocity and c = chord length. Fig 16 shows that the locus of local minimum lift coefficients in terms of reduced pitch rates is closely correlated with a delay time constant of $\tau = 3$. If this time delay constant is assumed to be a universal constant, the delayed reattachment angle can be estimated by

$$\alpha_{att} = \alpha_{fs} - \Delta\alpha_{att} = \alpha_{fs} - 343\, \alpha' c/2V \qquad \text{(deg)} \qquad (23)$$

where α_{fs} is the foil angle corresponding to C_{Lmin} or the beginning of the fully separated flow region for the steady flow condition.

CONCLUSIONS

With the propeller operating at the ship's stern, the propeller blade sections will encounter large spatial variations in angle of attack, especially in a maneuvering condition. Unsteady effects on the propeller side forces may not be small. A literature search is conducted to review the effect of unsteady motion on two-dimensional hydrodynamic forces.

A step change in angle of attack is shown to produce only half of the lift force at the instant of time when the change in angle of attack occurs. Steady lift is produced after the foil travels a distance of approximately 15 chord lengths. Forces computed using sectional airfoil data will be markedly different if unsteady coefficients are used instead of steady coefficients.

Depending on the instantaneous angle of attack, the flow on a hydrofoil surface exhibits different behavior. The flow phenomena are classified into several flow regimes. Each flow regime produces a different lift slope and hydrodynamic loading. The boundary of each flow regime is significantly altered by the unsteady motion. The physical phenomena associated with each flow regime are investigated in terms of reduced pitch rate and the instantaneous angle of attack. Methods to calculate the hydrodynamic loads in each flow regime are identified and presented in this report. The methods presented in this report are semi-empirical and should be improved with more rigorous methods such as RANS codes.

RECOMMENDATIONS

The present investigation has developed equations to predict dynamic lift for the different flow regimes. Equations need to be developed to predict dynamic drag and pitching moment, and the dynamic model needs to be implemented in the PFM code for predicting side forces.

The next phase of development involves improving the modeling of the physics. The following effects need to be evaluated for their importance, and modeled as necessary.

Reynolds number
Added mass
Camber, thickness, and leading edge profile shape
Cascade effects
Three-dimensional effects such as aspect ratio and sweep
Applicability of oscillating pitch data to the gust problem

Alternate methods for computing dynamic stall effects may provide additional insight. RANS calculations of dynamic stall could help evaluate the effects of Reynolds number scaling, profile geometry, and the relevance of oscillating pitch data to the gust problem. The analogy between fully separated flows and supercavitating flows could be evaluated by using the supercavitating flow theory of Widnall [28] as a means of computing foil forces and moments for extreme angles of attack.

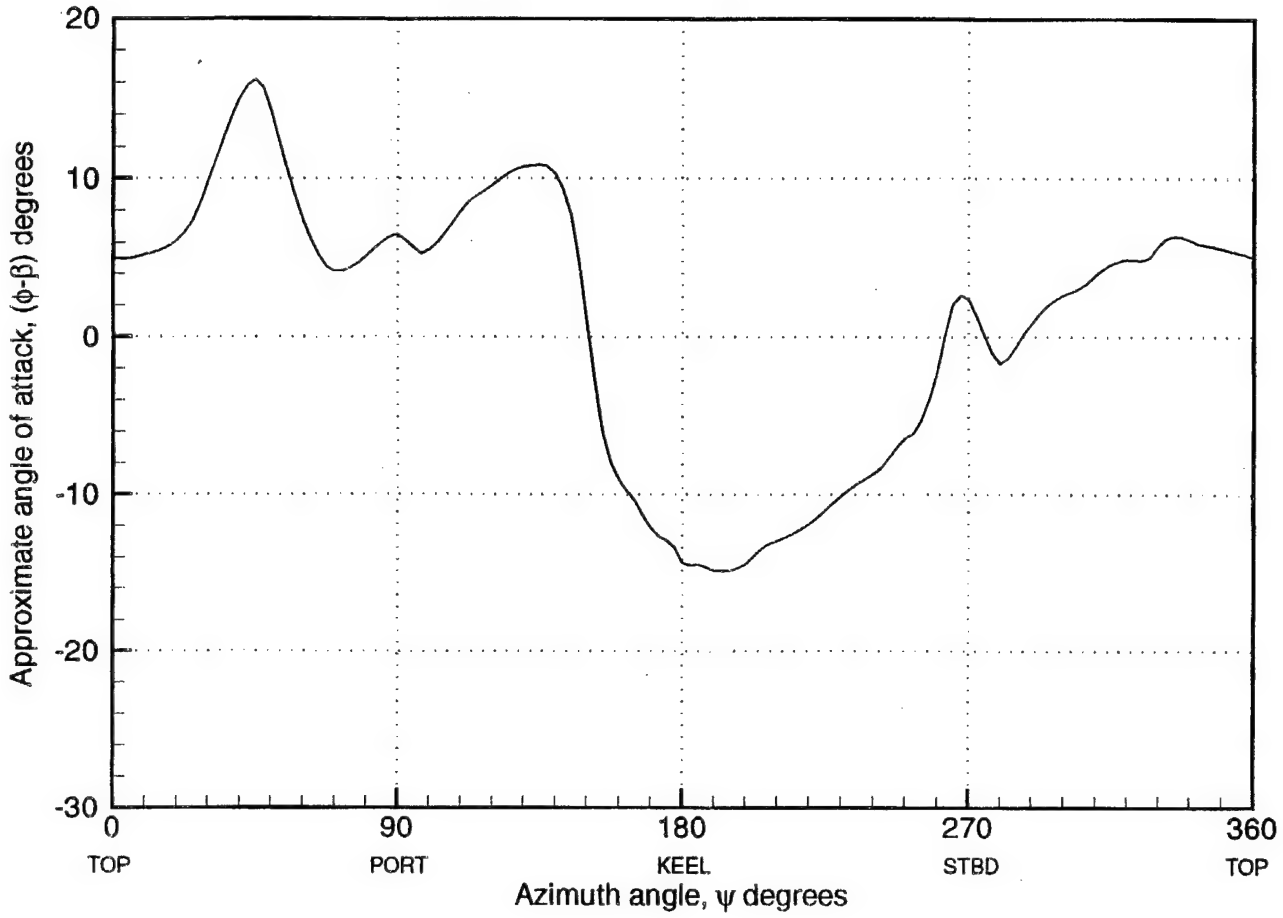

Fig 1. Inflow angles in the propeller plane at r/R=0.4 for a typical turn.

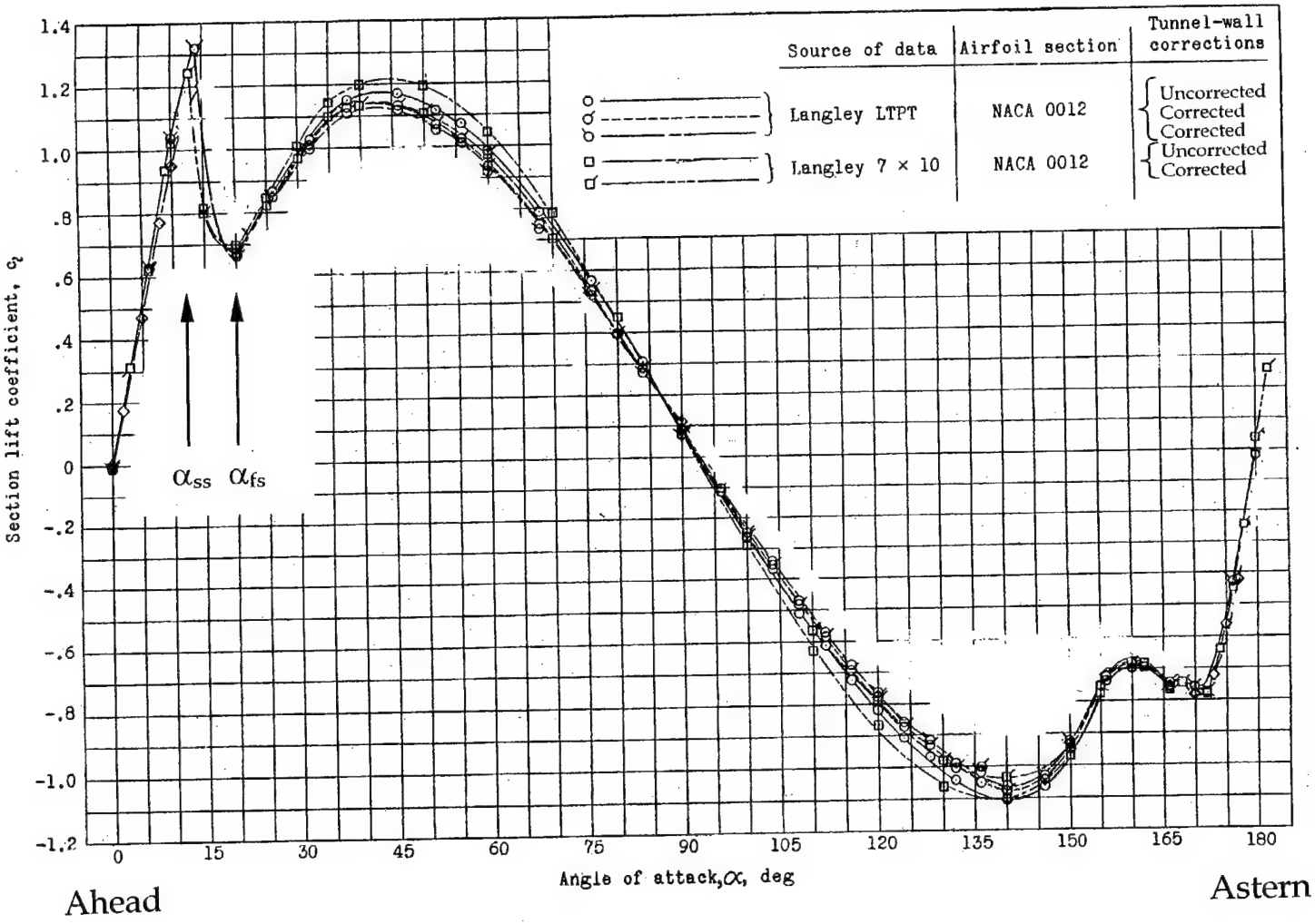

Fig 2a. Lift characteristics.

Fig 2. Lift and drag characteristics of the NACA 0012 profile [Ref 3].

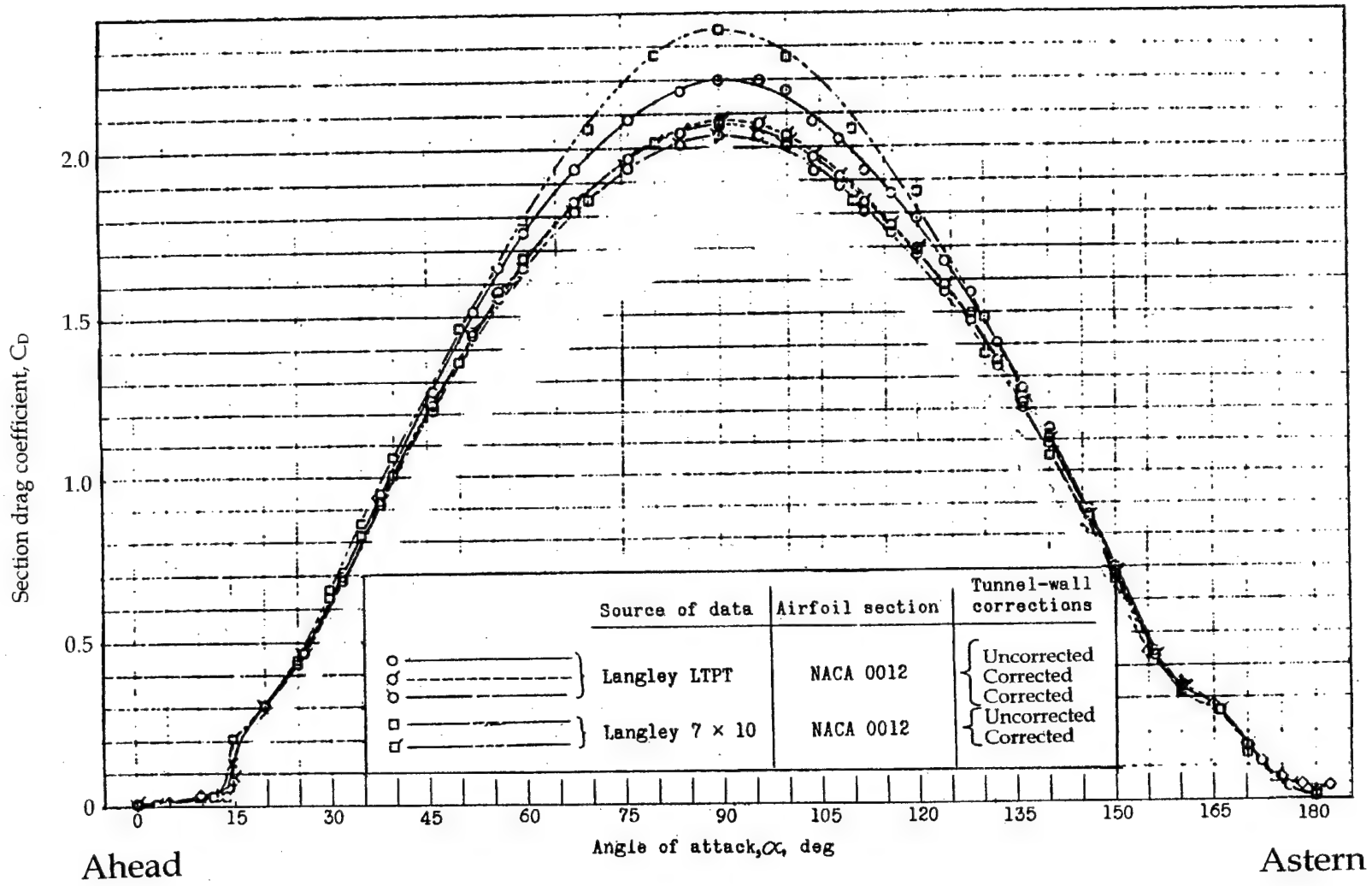

Fig 2b. Drag characteristics.

Fig 2. (Continued).

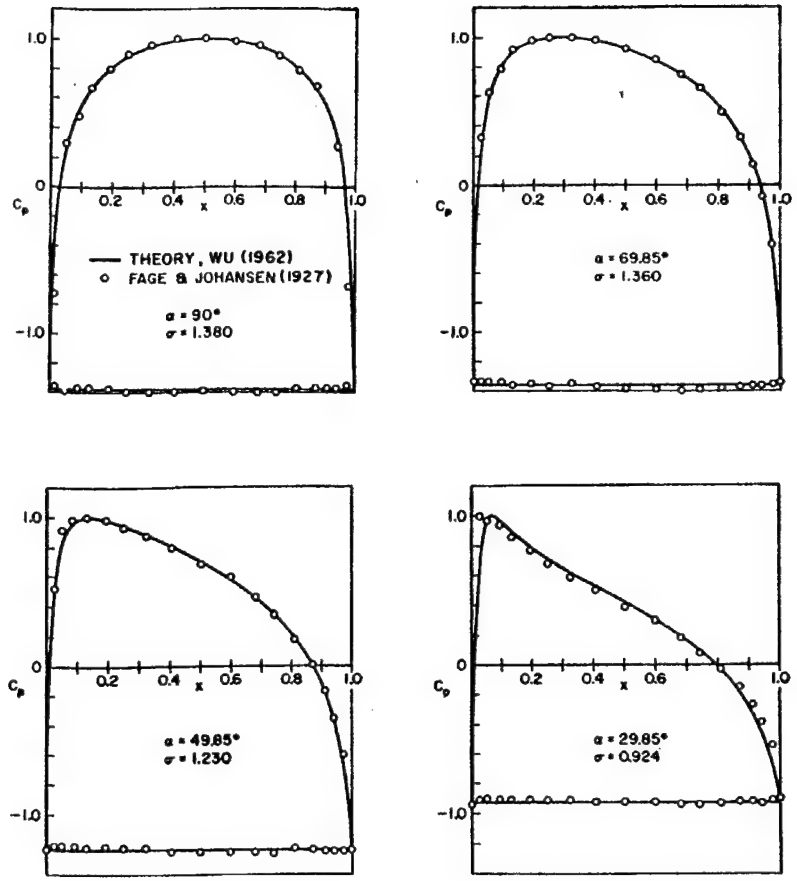

Fig 3. Pressure distributions on the wetted and separated sides of an oblique flat plate [Ref 5].

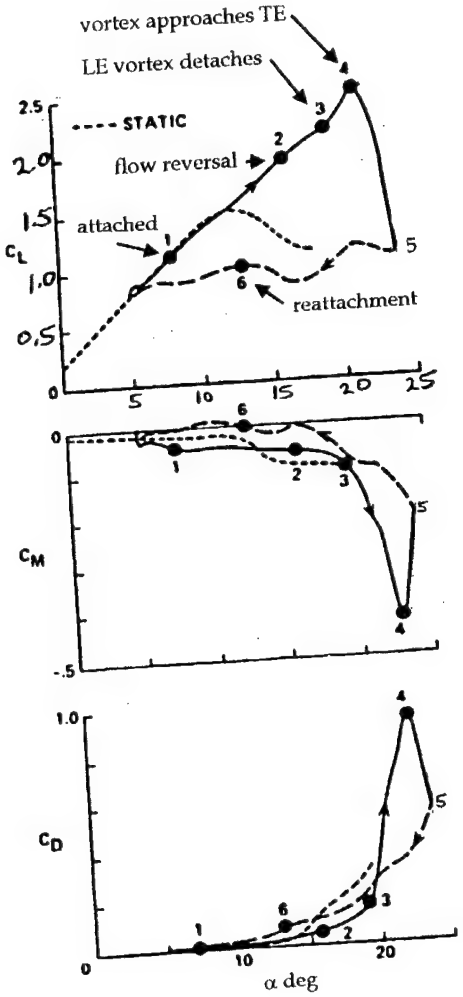

Fig 4. Dynamic stall events on the Vertol VR-7 airfoil at M_∞=0.25, α=15°+10°sinωt, and k=0.10 [Ref 10].

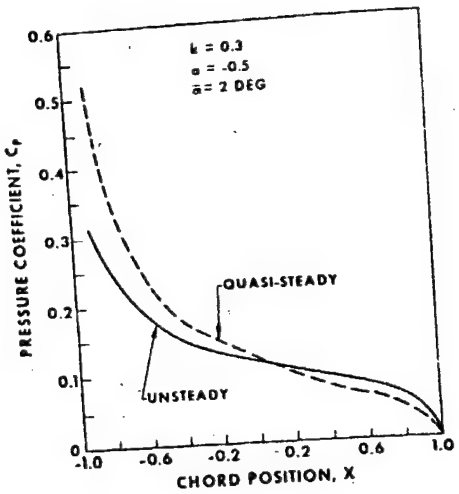

Fig 5. Instantaneous pressure distribution at $\omega t=11\pi/6$ [Ref 11].

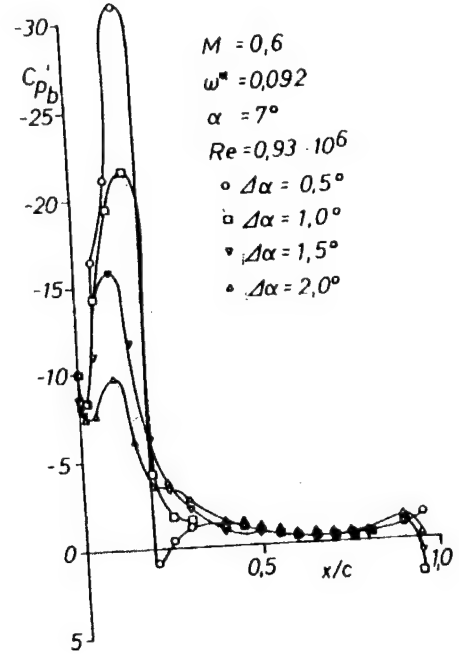

Fig 6. Effects of oscillation amplitude on the unsteady pressure distribution; M=0.6, α=7° [Ref 13].

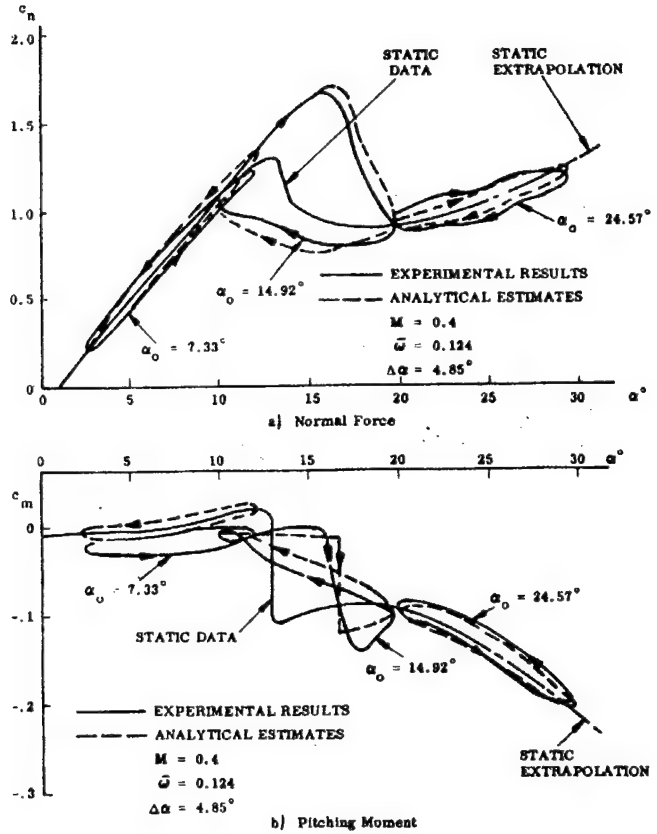

Fig 7. Effect of angle of attack on dynamic characteristics (Vertol 23010-1.58 airfoil section) [Ref 18].

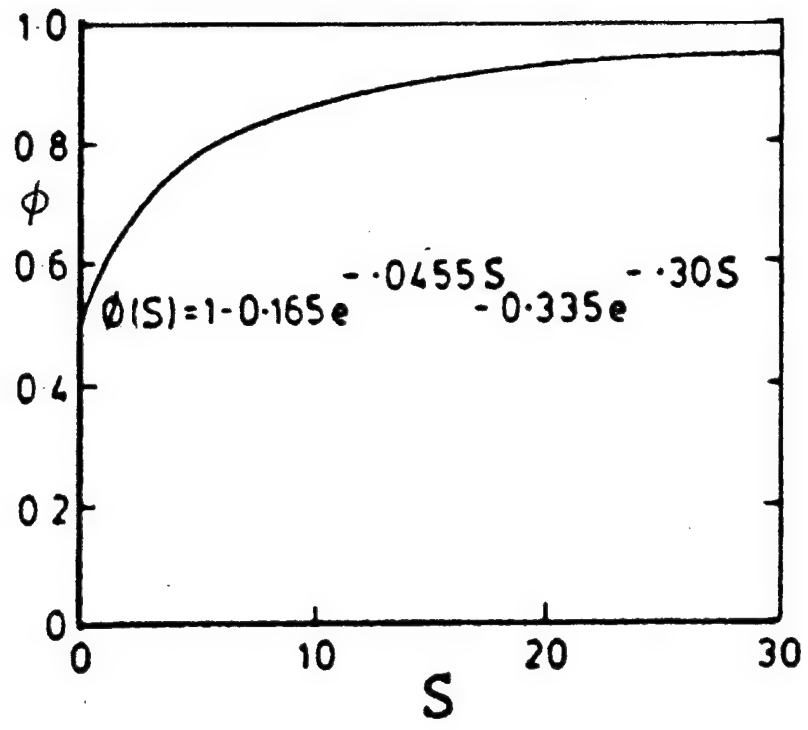

Fig 8. Wagner function [Ref 20].

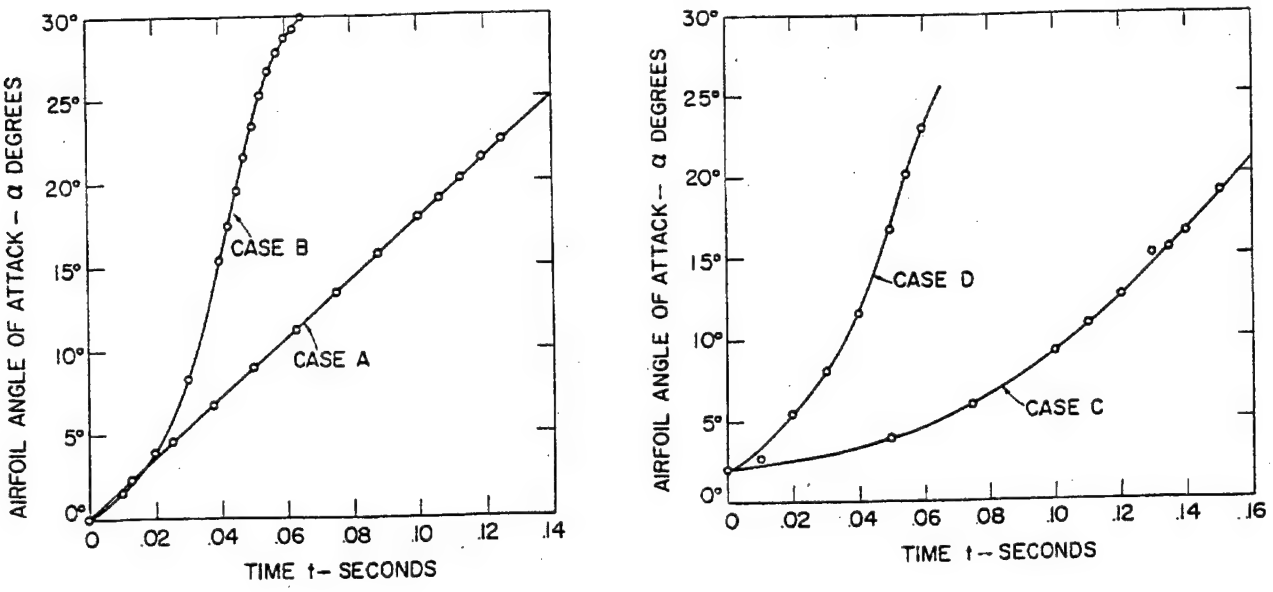

Fig 9a. Angle of attack.

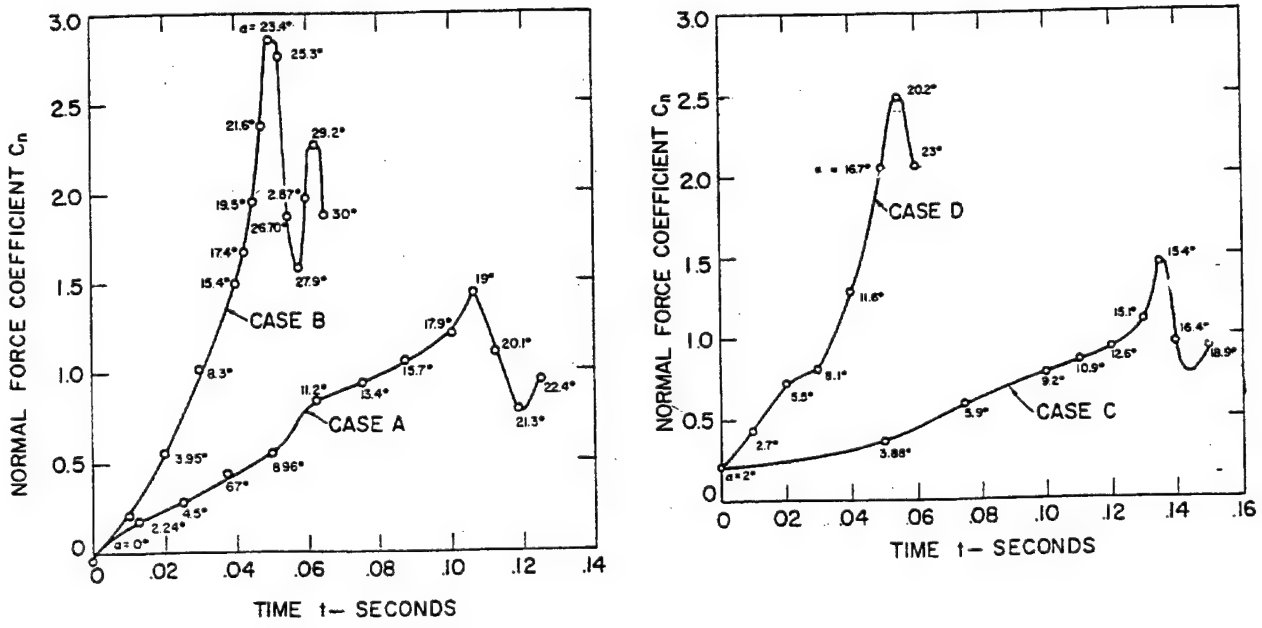

Fig 9b. Normal force coefficients.

Fig 9. Force response to the change of angle of attack [Ref 9].

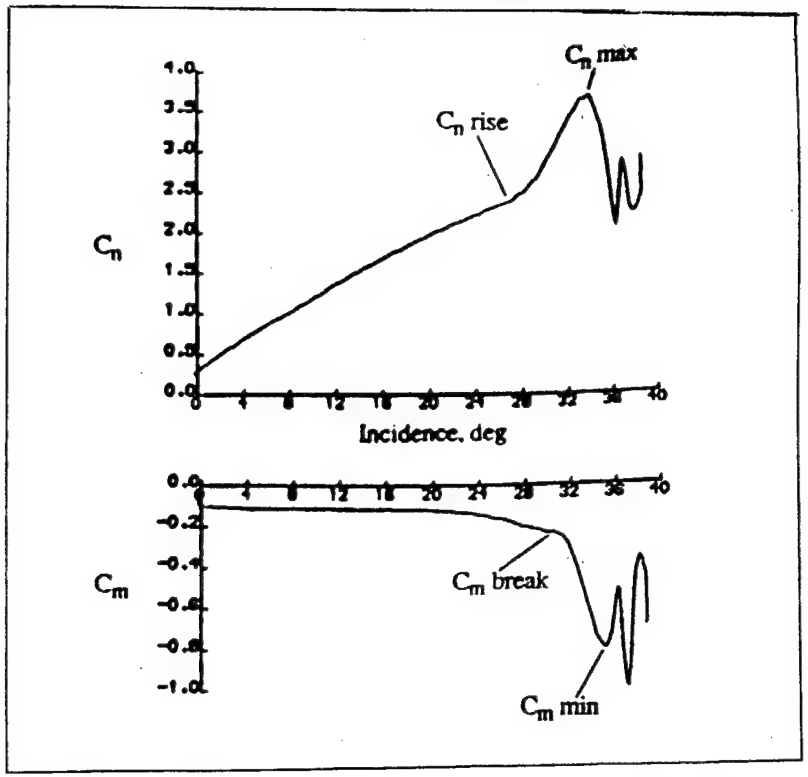

Fig 10. C_n and C_m as a function of incidence for the NACA 23012C performing a ramp-up motion from -1° to 40° at r=0.0332 [Ref 14].

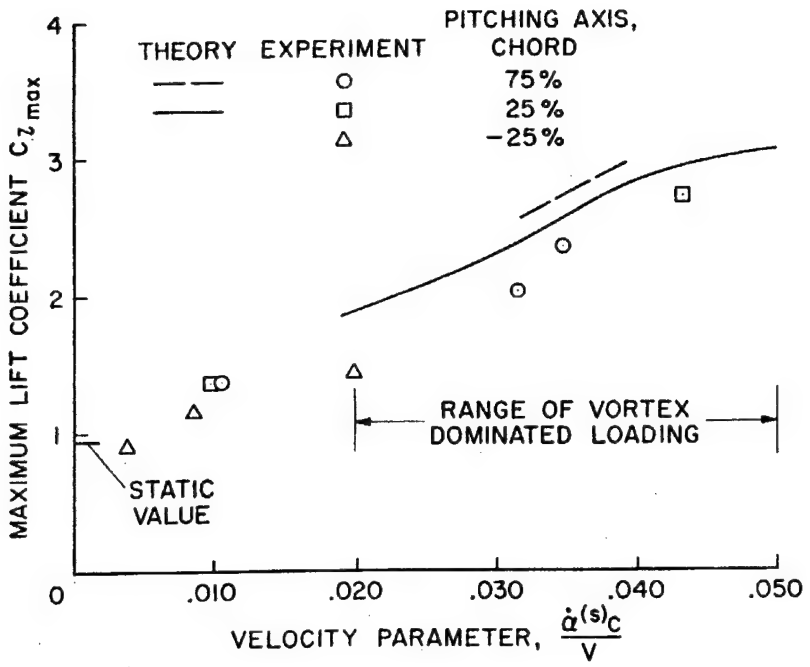

Fig 11. Maximum lift coefficient versus velocity parameter [Refs 25, 26].

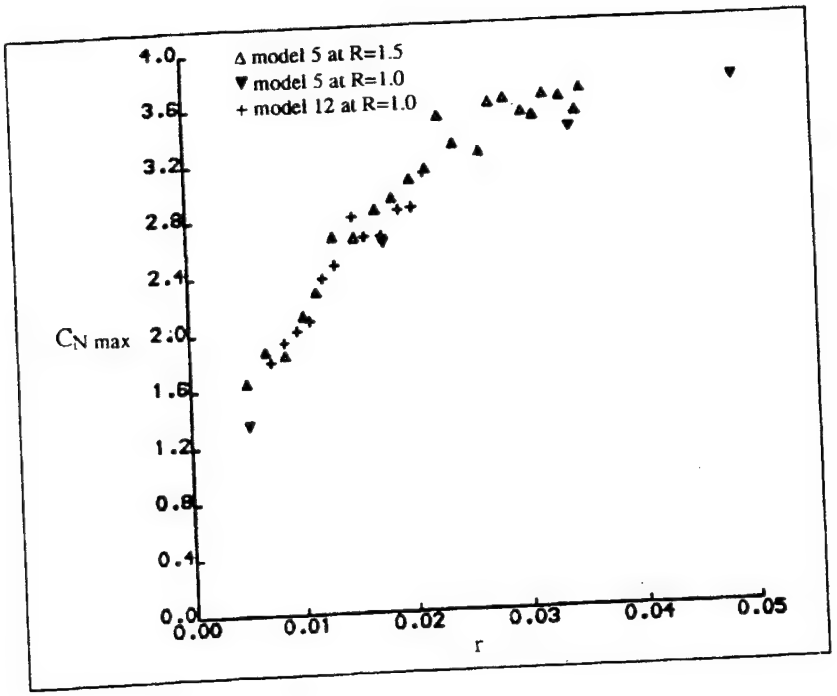

Fig 12. C_{Nmax} plotted against reduced pitch rate for ramp-up tests. Model 5 at R=1.5 and R=1.0, model 12 at R=1.0 [Ref 14].

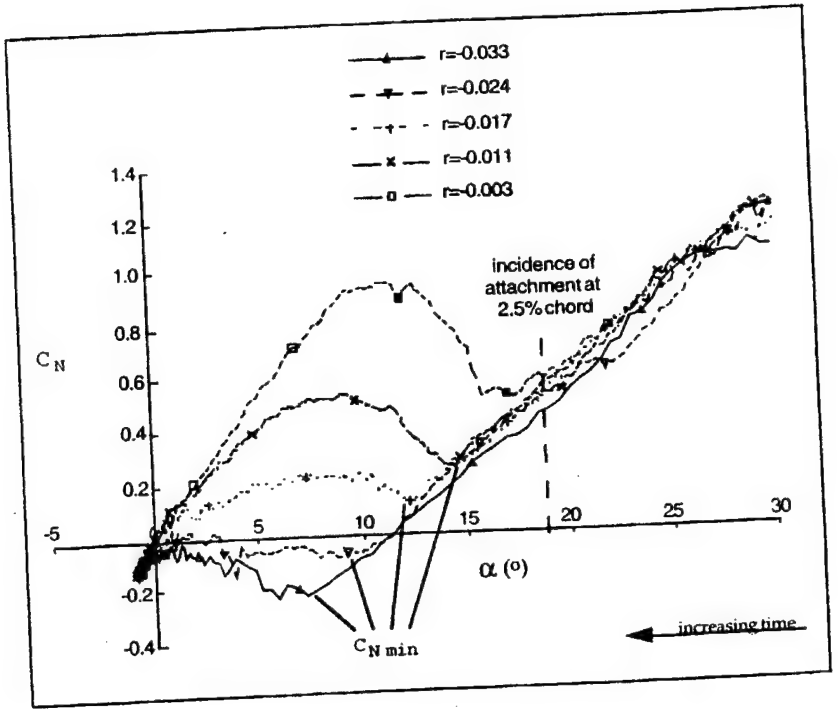

Fig 13. Plots of C_N versus α during 40° to -1° ramp-down tests of the NACA 0015 at $Re=1.5x10^6$. The effect of reduced pitch rate is shown. C_{Nmin} and the incidence of attachment at 2.5% chord are indicated. [Ref 27].

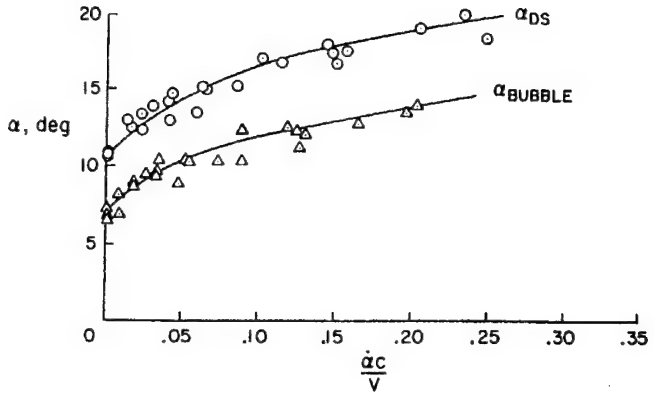

Fig 14. Delay characteristics of the angle of attack at which the bubble reattachment point moves forward of the 15 percent chord station (α_{bubble}), and the dynamic stall angle of attack (α_{DS}) (Reynolds number = 0.6 to 1.3x10^5). [Ref 19].

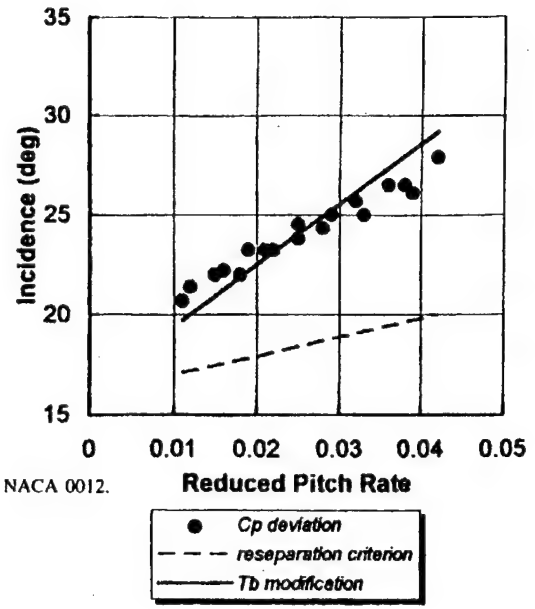

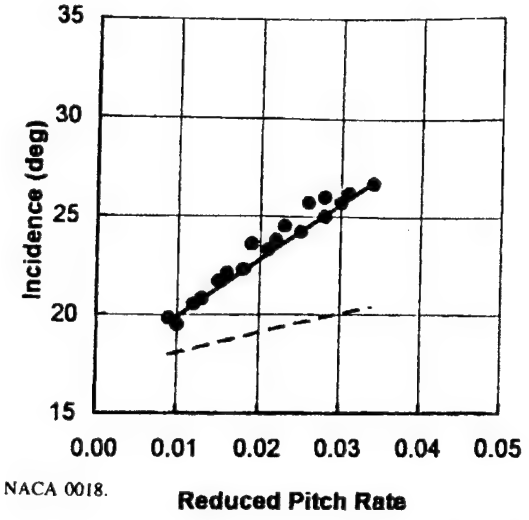

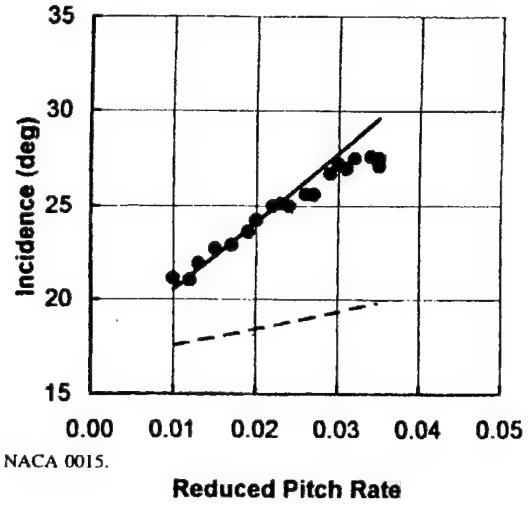

Fig 15a. Symmetric foils.

Fig 15. Inception of dynamic moment stall angle vs reduced pitch rate [Ref 15].

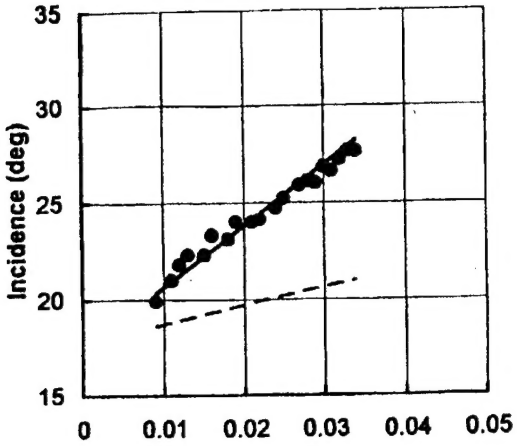

NACA 23012C.

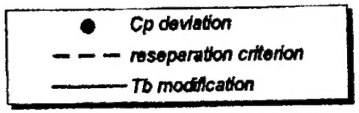

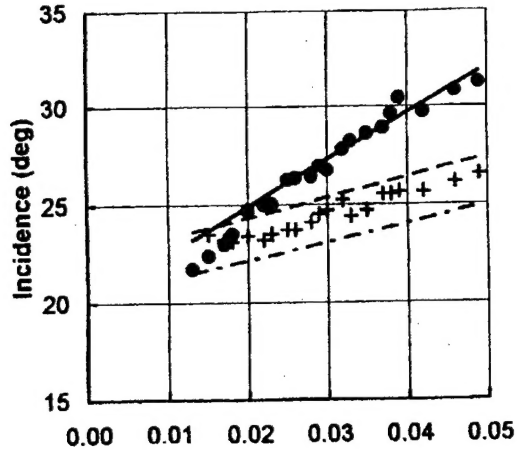

NACA 23012B.

Fig 15b. Cambered foils.

Fig 15. (Continued).

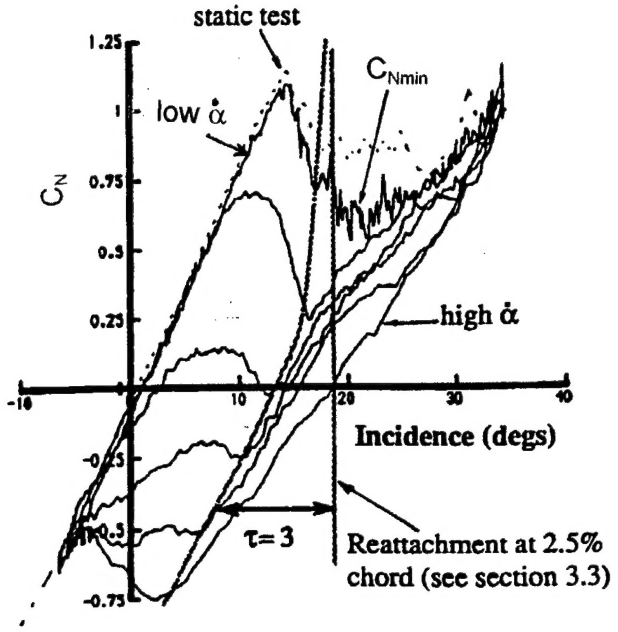

Fig 16. Normal force coefficient versus incidence for a range of pitch rates [Ref 34].

REFERENCES

1. Abbott I. H. and A. E. von Doenhoff, Theory of Wing Sections, Dover Publications, Inc, New York, 1959
2. Shen, Y. T. and R. Eppler, " Wing Sections for Hydrofoils - Part 2 Nonsymmetrical Profiles", J of Ship Research, Sept. 1981 pp 191-200
3. Critzos C., H. Heyson, and R. Boswinkle, "Aerodynamic Characteristics of NACA 0012 Airfoil Section at Angles of Attack from 0 to 180 deg," NACA TN 3361 Jan. 1955
4. McCroskey, W. J., et all, "Dynamic stall on Advanced Airfoil Sections", J. of American Helicopter Society, Vol 26, no 3, July 1981, pp 40-50
5. Wu, Yao-Tsu., "Cavity and Wake Flows", Annual Review of Fluid Mechanics, Vol 4, 1972
6. Bisplinhoff R., Ashley, H. and R. Halfman, Aeroelasticity, Addison-Wesley, 1955
7. Theodorsen, T., "General Theory of Aerodynamic Instability and the Mechanism of Flutter," NACA Report 496, 1935
8. Ham, N. D. and M. S. Garelick, "Dynamic Stall Considerations in Helicopter Rotors," J. of American Helicopter Society, Vol 13, no 2, April 1968 pp 49-55
9. Kramer, M., "Increase in the Maximum Lift of an Airplane Wing due to a sudden Increase in its Effective Angle of Attack," NACA TM. 678, 1932
10. McCroskey, W. J., "The Phenomenon of Dynamic Stall," NASA TM 81264 March 1981
11. Carta, F., "Effect of Unsteady Pressure Gradient Reduction on Dynamic Stall Delay" AIAA Journal of Aircraft, Oct 1971, Vol 8 pp 839-841]
12. Shen Y. and F. Peterson, "Unsteady Cavitation on an Oscillating Hydrofoil," 12th ONR Naval Hydrodynamics Symposium, Wash. D. C., 1978
13. Triebstein H. "Steady and Unsteady Pressure Distributions on a NACA 0012 Profile in Separated Transonic Flow" ICAS -84-1.5.1,
14. Green R., Galbraith R. and A. Niven, "Measurements of the dynamic stall vortex convection speed," Aeronautical Journal, Oct 1992, pp 319-325
15. Niven, A. J. and R. A. Galbraith, "Modeling dynamic stall vortex inception at low Mach numbers," The Aeronautical J., Feb 1997 , pp 67-76
16. Telionis, D. P. "Review-Unsteady Boundary Layers, Separated and Attached", J of fluids Engineering, March 1979, Vol 101 pp 29-41
17. Shen Y. and F. Peterson, "The Influence of Hydrofoil Oscillation on Boundary Layer Transition and Cavitation Noise," 13th ONR Naval Hydrodynamics Symposium, Tokyo, Japan, 1980
18. Ericsson, L. E. and Reding, J. P., "Dynamic Stall Simulation Problems," J. of Aircraft, Vol 8 , no 7, July 1971, pp 579-583
19. Johnson W. and N. D. Ham, "On the Mechanism of Dynamic Stall", Journal of the American Helicopter Society Vol 17, no 4, Oct 1972, pp 36-45
20. Bielawa, R. L., Rotary Wing Structural Dynamics and Aeroelasticity , AIAA Education Series, Washington DC , 1992
21. Beddoes T. S., "A Synthesis of Unsteady Aerodynamic Effects Including Stall Hysteresis," Vertica, 1976, Vol 1 pp 113-123
22. Beddoes T. S., "Onset of Leading Edge Separation Effects under Dynamic Conditions and Low Mach Number," American Helicopter Society Annual Forum 1978
23. Gangwani, S. T., "Synthesized Airfoil Data Method for Prediction of Dynamic Stall and Unsteady Airloads," Proceeding of the 39th Annual Forum of the American Helicopter Society, 1983. See NASA Contractor Report 3672 for more details.
24. Green R., and R. A. Galbraith, "A Demonstration of the Effect of the Testing Environment

on Unsteady Aerodynamics Experiments," Aeronautical Journal, March 1994
25. Johnson W., "The Response and Airloading of Helicopter Rotor Blades due to Dynamic Stall," MIT, ASRL TR 130-1 May 1970
26. Johnson W., "A Comprehensive Analytical Model of Rotorcraft Aerodynamics and Dynamics," Camrad/JA user manual, Johnson Aeronautics, Palo Alto, Ca.
27. Green R., and R. A. Galbraith, "Phenomena Observed during Aerofoil Ramp-down Motions from the fully Separated State," Aeronautical Journal, Nov. 1994
28. Widnall, S. E., "Unsteady Loads on Hydrofoils Including Free Surface Effects and Cavitation," MIT FDRL Report 64-2, 1964
29. Carta F., "A theoretical study of the Effect of Unsteady Pressure Gradient Reduction on Dynamic Stall Delay", Proceeding of Fluid Dynamics of Unsteady Three-dimensional and Separated Flows," Georgia Institute of Tech. June 1971,
30. Ericsson, L. E. and Reding, J. P., "Dynamic Stall at High Frequency and Large Amplitude," J. of Aircraft, Vol 17, no 3, 1980, pp 136-142
31. Tran C. T. and Petot, D., "Semi-empirical Model for the Dynamic Stall of Airfoils in View of the Application to the Calculation of Responses of a Helicopter Blade in Forward Flight", Paper #48, Sixth European Rotorcraft and Powered -Lift aircraft Forum, Bristol, England, 1980
32. Gormont, R. E., "A Mathematical Model of Unsteady Aerodynamics and Radial Flow for Application to Helicopter Rotors," US Army AMRDL Eustis Directorate Report TR-72-67, 1973
33. Leishman, J. G. and T. S. Beddoes, " A Semi-empirical Model for Dynamic stall," J. of the American Helicopter Society, July 1989, pp 3-17
34. Niven A. J., R. A. Galbraith and G. F. Herring, " Analysis of Reattachment during Ramp Down Tests," Vertica, Vol 13, no 2, 1989, pp 187-196
35. Fung, Y. C., An Introduction to the Theory of Aeroelasticity, Dover Publications Inc., New York, 1993